A comparison of particle and fluid models for positive streamer discharges in air

Zhen Wang[1,2], Anbang Sun[1], Jannis Teunissen[2]

[1]State Key Laboratory of Electrical Insulation and Power Equipment, School of Electrical Engineering, Xi'an Jiaotong University, Xi'an, 710049, China,
[2]Centrum Wiskunde & Informatica, Amsterdam, The Netherlands

E-mail: `jannis.teunissen@cwi.nl`, `anbang.sun@xjtu.edu.cn`

Abstract. Both fluid and particle models are commonly used to simulate streamer discharges. In this paper, we quantitatively study the agreement between these approaches for axisymmetric and 3D simulations of positive streamers in air. We use a drift-diffusion-reaction fluid model with the local field approximation and a PIC-MCC (particle-in-cell, Monte Carlo collision) particle model. The simulations are performed at 300 K and 1 bar in a 10 mm plate-plate gap with a 2 mm needle electrode. Applied voltages between 11.7 and 15.6 kV are used, which correspond to background fields of about 15 to 20 kV/cm. Streamer properties like maximal electric field, head position and velocity are compared as a function of time or space.

Our results show good agreement between the particle and fluid simulations, in contrast to some earlier comparisons that were carried out in 1D or for negative streamers. To quantify discrepancies between the models, we mainly look at streamer velocities as a function of streamer length. For the test cases considered here, the mean deviation in streamer velocity between the particle and fluid simulations is less than 4%. We study the effect of different types of transport data for the fluid model, and find that flux coefficients lead to good agreement whereas bulk coefficients do not. Furthermore, we find that with a two-term Boltzmann solver, data should be computed using a temporal growth model for the best agreement. The numerical convergence of the particle and fluid models is also studied. In fluid simulations the streamer velocity increases somewhat using finer grids, whereas the particle simulations are less sensitive to the grid. Photoionization is the dominant source of stochastic fluctuations in our simulations. When the same stochastic photoionization model is used, particle and fluid simulations exhibit similar fluctuations.

1. Introduction

Streamer discharges are elongated conducting channels that typically appear when an insulating medium is locally exposed to a field above its breakdown value [1]. Electric field enhancement around their tips causes streamers to rapidly grow through electron impact ionization. Due to this field enhancement, they can propagate into regions in which the background field was initially below breakdown. Streamers occur in nature as sprites [2, 3] and they are used in diverse applications such as the production of radicals [4], pollution control [5], the treatment of liquids [6], plasma medicine [7], and plasma combustion [8].

Over the last decades, numerical simulations have become a powerful tool to study streamer physics and to explain experimental results. Two types of models have commonly been used: particle models (e.g., [9–13]) and fluid models (e.g., [14–20]).

Particle models track the evolution of a large number of electrons, represented as (super-)particles, and other relevant species. They can be used to study stochastic phenomena such as electron runaway or discharge inception. Another advantage of such models is that no assumptions on the EVDF (electron velocity distribution function) need to be made. In fluid models all relevant species are approximated by densities, which can greatly reduce computational costs. These densities evolve due to fluxes and source terms, which are computed by making certain assumptions about the EVDF. Common is the local field approximation, in which it is assumed that electrons are instantaneously relaxed to the local electric field. Higher-order fluid models can also be used [21, 22]. In principle, it would even be possible to solve the underlying spatio-temporal Boltzmann equation [23, 24], but this is at present computationally infeasible for multi-dimensional streamer simulations.

Both particle models and fluid models with the local field approximation have frequently been used to study positive streamer discharges. Although it is well known that the local field approximation can lead to errors [25, 26], it is not clear how significant these errors are for the modeling of positive streamers. The first goal of this paper is therefore to study the agreement between particle and fluid simulations of positive streamers in air, using both axisymmetric and 3D simulations. We use a standard particle model of the PIC-MCC (particle-in-cell, Monte Carlo

collision) type and a standard drift-diffusion reactions fluid model with the local field approximation.

When comparing models, it is important to have consistent input data computed from the same electron-neutral cross sections. However, transport coefficients for a fluid model can be computed with different types of Boltzmann solvers, and both so-called *flux* and *bulk* coefficients can be computed. Bulk coefficients describe the dynamics of a group of electrons, whereas flux coefficients characterize the properties of individual electrons [21, 27]. Although the use of flux coefficients is generally recommended for plasma modeling [21, 28], it is not fully clear how the use of bulk data affects simulations of positive streamers [29]. Furthermore, with a two-term Boltzmann solver it possible to use either a spatial or temporal growth model, which lead to different transport coefficients [30]. The second goal of this paper is therefore to determine the most suitable type of transport data for use in fluid simulations of positive streamers.

Past work Below, we briefly discuss some of the past work on the comparison of particle and fluid models for streamer discharges. In [29], four models were compared by simulating a short negative streamer in 3D: a particle model, the 'classical' fluid model with the local field approximation, an extended fluid model, and a hybrid particle-fluid model. These simulations were carried out in a 1.2 mm gap using a background electric field well above breakdown, without taking photoionization into account. The classical fluid model here deviated from the other models in terms of streamer velocity and shape, but this was probably due to an implementation flaw that was later found. In [31] three plasma fluid models of different order were compared against particle simulations for planar ionization waves, which can be thought of as "1D" negative streamers. The classical fluid model was found to give rather reasonable results, somewhat in contrast with the conclusions of [26]. Finally, in [32] six streamer codes from different groups were benchmarked against each other, aiming towards model verification. All codes implemented the classical fluid model, and three test cases with positive streamers were considered. Good agreement was found on sufficiently fine grids, and with corresponding small time steps.

Particle and fluid models have also been compared for other types of discharges. In [33] particle, fluid

and hybrid models were benchmarked against each other and against experimental data. This review paper focused on applications related to plasma display panels, capacitively coupled plasmas and inductivetly coupled plasmas. The authors conclude that "*Excellent agreement can be found in these systems when the correct model is used for the simulation. Choosing the right model requires an understanding of the capabilities and limitations of the models and of the main physics governing a particular discharge.*". Furthermore, in [34], particle and fluid models were compared for capacitively and inductively coupled argon-oxygen plasmas, in [35] they were compared for atmospheric pressure helium microdischarges, and in [36] they were extensively compared for low-pressure ccrf discharges.

In contrast to the above work, we here compare multidimensional particle and fluid simulations of positive streamers in air, propagating in background fields below breakdown, including photoionization. The paper is organized as follows. In section 2, the particle and fluid models are described as well as the simulation conditions. In section 3.1, we first compare axisymmetric and 3D particle and fluid simulations of positive streamers in air, after which the influence of transport data is studied with axisymmetric fluid simulations in section 3.2. We then investigate the numerical convergence of both types of models in section 3.3, and we determine the dominant source of stochastic fluctuations in the particle simulations in section 3.4. Finally, in section 3.5, the models are again compared for different applied voltages.

2. Model description

The particle and fluid models are briefly introduced below, after which the simulation conditions, photoionization and the adaptive mesh are described. We use both axisymmetric and 3D models. For brevity, axisymmetric models will sometimes be referred to as "2D".

Due to the short time scales considered in this paper, ions are assumed to be immobile in both the particle and fluid models. Information about the computational cost of simulations is given in Appendix A.

2.1. Particle (PIC-MCC) model

We use a PIC-MCC (particle-in-cell, Monte-Carlo Collision) model that combines the particle model described in [10] with the Afivo AMR (adaptive mesh refinement) framework described in [37]. Electrons are tracked as particles, ions as densities, and neutrals as a background that electrons stochastically collide

with. Below, we briefly introduce the model's main components.

2.1.1. Particle mover and collisions The coordinates $\vec{x}$ and velocities $\vec{v}$ of simulated electrons are advanced with the 'velocity Verlet' scheme described in [10]:

$$\vec{x}(t + \Delta t) = \vec{x}(t) + \Delta t\, \vec{v}(t) + \frac{1}{2}\Delta t^2\, \vec{a}(t), \qquad (1)$$

$$\vec{v}(t + \Delta t) = \vec{v}(t) + \frac{1}{2}\left[\vec{a}(t) + \vec{a}(t + \Delta t)\right], \qquad (2)$$

where $\vec{a} = -(e/m_e)\vec{E}$ is the acceleration due to the electric field $\vec{E}$, and e is the elementary charge and m_e the electron mass.

In axisymmetric simulations particles are evolved as in a 3D Cartesian geometry. However, their acceleration, which is due to an axisymmetric field, is projected onto a radial and axial components before it is used. The acceleration in equation (1) is then given by $\vec{a} = (a_r\, x/r, a_r\, y/r, a_z)$, where x and y denote the two (3D) particle coordinates corresponding to the radial direction and $r = \sqrt{x^2 + y^2}$. In equation (2), the radial velocity is updated as

$$\vec{v}_{x,y}(t + \Delta t) = \vec{v}_{x,y}(t) + \frac{1}{2}\hat{r}\left[a_r(t) + a_r(t + \Delta t)\right],$$

where $\hat{r} = (x, y)/r$.

Electron-neutral collisions are handled with the null-collision method [10, 38], using collision rates calculated from cross section input data.

2.1.2. Super-particles Due to the large number of electrons in a streamer discharge, it is generally not feasible to simulate all electrons individually. Instead, so-called "super-particles" are used, whose weights w_i determine how many physical particles they represent [39]. The procedure followed here is similar to that in [10]. A parameter N_{ppc} controls the 'desired' number of particles per grid cell. We use $N_{ppc} = 75$, except for section 3.4, in which it is varied. The desired particle weights ω are then determined as

$$\omega = n_e \times \Delta V / N_{ppc} \qquad (3)$$

where n_e is the electron density in a cell and ΔV the cell volume. Furthermore, the minimum particle weight is $\omega_{\min} = 1$.

Particle weights are updated when the number of simulations particles has grown by a factor of 1.25, after the AMR mesh has changed, or after 10 time steps in axisymmetric simulations (see below). The particles in a cell for which $w_i < (2/3) \times \omega$ are merged, by combining two such particles that are close in energy into one with the sum of the original weights. The coordinates and velocity of the merged particle are randomly selected from one of the original particles, see [40]. Particles are split when $w_i > (3/2) \times \omega$. Their
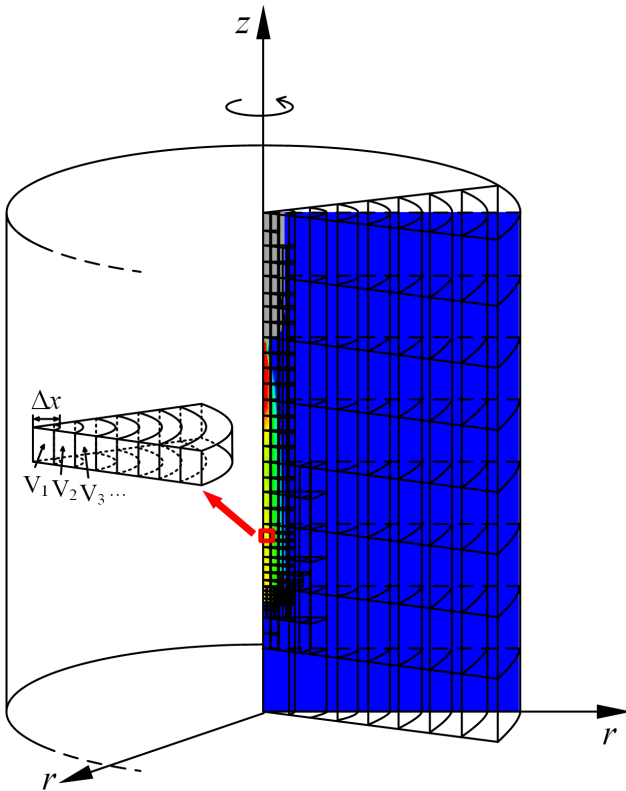
Figure 1: Illustration of the adaptive mesh in an axisymmetric streamer simulation, also showing the electron density. The grid is coarser than in an actual simulation. The enlarged view illustrates the relation between cell volumes and radius.

weight is then halved after which identical copies of these particles are added, which will soon deviate from them due to the random collisions.

In axisymmetric simulations particle weights are updated every ten time steps to reduce fluctuations near the axis. Figure 1 illustrates an axisymmetric mesh in which cell volumes depend on the radial coordinate as $\Delta V = 2\pi r \Delta r \Delta z$. Cells with small volumes contain fewer physical electrons, and because the minimal super-particle weight is one, stochastic fluctuations in such cells are larger. Furthermore, super-particle weights given by equation (3) are proportional to the cell volume. Particles with high weights can therefore cause significant fluctuations when they move towards the axis. We update the particle weights more frequently in axisymmetric simulations to limit these fluctuations.

2.1.3. Mapping particles to the grid Particles are mapped to grid densities using a standard bilinear or trilinear weighting scheme, as in [10]. Near refinement boundaries, the mapping is locally changed to the

"nearest grid point" (NGP) scheme, to ensure that particle densities are conserved. In axisymmetric coordinates the mapping is also done using bilinear weighting, but the radial variation in cell volumes is taken into account. The interpolation of the electric field from the grid to particles is done using standard bilinear (2D) or trilinear (3D) interpolation. Note that there are more advanced weighting schemes for handling axisymmetric coordinates systems [41], but these approaches are challenging to combine with the cell-centered AMR used in our models.

2.1.4. Temporal discretization We use the following CFL-like condition

$$\Delta t_{\text{cfl}}\,\tilde{v}_{\max} \leq 0.5 \times \Delta x_{\min}, \tag{4}$$

where $\Delta x_{\min}$ indicates the minimum grid spacing, and $\tilde{v}_{\max}$ is an estimate of the particle velocity at the 90%-quantile. This prevents a few fast particles from affecting Δt_{cfl}.

Another time step constraint is the Maxwell time, also known as the dielectric relaxation time, which is a typical time scale for electric screening:

$$\Delta t_{\text{drt}} = \varepsilon_0 / \left(e n_{e,\max}\,\mu_e\right), \tag{5}$$

where ε_0 is the dielectric permittivity, $n_{e,\max}$ is the maximal electron density, and μ_e the electron mobility, as determined in the local field approximation (see section 2.2.2).

The actual time step is then the minimum of Δt_{cfl} and Δt_{drt}, and it is furthermore adjusted such that the number of electrons does not grow by more than 20% between time steps.

2.1.5. Input data We use Phelps' cross sections for N_2 and O_2 [42, 43]. These cross sections contain a so-called *effective* momentum transfer cross sections, which account for the combined effect of elastic and inelastic processes [44]. To use them in particle simulations, we convert them to elastic cross sections by subtracting the sum of the inelastic cross sections. This is an approximate procedure, but the resulting cross sections are suitable for a model comparison.

2.2. Fluid model

We use a drift-diffusion-reaction fluid model with the local field approximation, as implemented in [15]. The electron density n_e evolves in time as

$$\partial_t n_e = \nabla \cdot (n_e \mu_e \mathbf{E} + D_e \nabla n_e) + S_R + S_{ph} \tag{6}$$

where μ_e and D_e indicate the electron mobility and the diffusion coefficient, S_{ph} is the non-local photoionization source term (see section 2.4), and S_R

is a source term due to the following ionization and attachment reactions:

$$e + N_2 \longrightarrow 2e + N_2^+ \ (15.60 \text{ eV})$$
$$e + N_2 \longrightarrow 2e + N_2^+ \ (18.80 \text{ eV})$$
$$e + O_2 \longrightarrow 2e + O_2^+$$
$$e + 2O_2 \longrightarrow O_2^- + O_2$$
$$e + O_2 \longrightarrow O^- + O$$
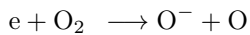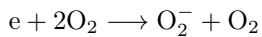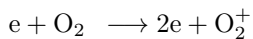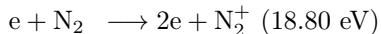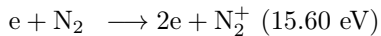
Ion densities also change due to the above reactions. Transport coefficients and reaction rates are determined using the local field approximation, see section 2.2.2.

2.2.1. Time integration Advective electron fluxes are computed using the Koren flux limiter [45] and diffusive fluxes using central differences, see [15] for details. Time integration is performed with Heun's method, a second order accurate explicit Runge-Kutta scheme. Time steps are limited according to the following restrictions:

$$\Delta t_{\text{cfl}} \left(\frac{2N_{\text{dim}}}{\Delta x^2} + \sum \frac{v_i}{\Delta x} \right) \leq 0.5,$$
$$\Delta t_{\text{drt}} \left(e n_e \mu_e / \varepsilon_0 \right) \leq 1,$$
$$\Delta t = 0.9 \times \min(\Delta t_{\text{drt}}, \Delta t_{\text{cfl}}),$$

where Δt_{cfl} corresponds to a CFL condition (including diffusion), Δt_{drt} corresponds to the dielectric relaxation time (as in equation (5)), N_{dim} is the dimensionality of the simulation, Δt is the actual time step used, and Δx stands for the grid spacing, which is here equal in all directions.

2.2.2. Input data The fluid model requires tables of transport and reaction data versus electric field strength as input. We use two methods to compute such data from the cross sections that were also used for the PIC model, see section 2.1.5. The first is BOLSIG+, which is a widely used two-term Boltzmann solver [30, 46]. When the electron velocity distribution is strongly anisotropic, for example in high electric fields, the use of the two term approximation can introduce errors [47]. The second method we use is a Monte Carlo swarm code `gitlab.com/MD-CWI-NL/particle_swarm`, similar to e.g. [48, 49]. The basic idea of this approach is to trace electrons in a uniform field, from which transport and reactions coefficients can be obtained.

With the Monte Carlo method we compute both so-called *flux* and *bulk* coefficients [21, 27]. Flux data describes the average properties of individual electrons, whereas bulk data describes average properties of a group of electrons, taking non-conservative collisions such as ionization and attachment into account. Consider for example a group of electrons, which

changes in size due to non-conservative collisions. The bulk drift velocity then describes the average velocity of the center of mass of this group, whereas the flux drift velocity describes the average velocity of individual electrons. These two definitions differ when the probability of non-conservative collisions is not uniform in space, which causes motion of the center of mass.

One of the main differences between bulk and flux data is that in high fields the bulk mobility is higher than the flux mobility, as shown in figure 7. Unless mentioned otherwise, the fluid simulations presented in this paper use Monte Carlo flux data.

2.3. Computational domain and initial conditions

Simulations are performed in artificial air, containing 80% N_2 and 20% O_2, at $p = 1$ bar and $T = 300$ K. We will give electric fields in units of kV/cm. With a gas number density of $N = 2.414 \times 10^{25}$ m^{-3}, assuming the ideal gas law, 1 kV/cm corresponds to about 4.14 Td (Townsends).

The computational domain used for the comparison of cylindrical models is shown in figure 2. It measures 10 mm in both the axial and radial directions. For the 3D Cartesian simulations, a similar domain of 20 mm × 20 mm × 10 mm is used. A rod-shaped electrode with a semi-spherical cap is placed at center of the domain. This electrode is 2.0 mm long and has a radius of 0.2 mm.

For the electric potential, Dirichlet boundary conditions are applied to the lower and upper domain boundaries, and a homogeneous Neumann boundary condition is applied on the other boundaries. In terms of electrostatics the axisymmetric and 3D simulations are not fully equivalent, because of the different geometry in which these boundary conditions are applied.

For the electron density homogeneous Neumann conditions are applied on all domain boundaries, except for the rod electrode. The electrode absorbs electrons but does not emit them. Since a positive voltage is applied on this electrode, secondary electron emission was not taken into account.

There is initially no background ionization besides an electrically neutral plasma seed that is placed at the tip of the electrode. This seeds helps to start discharges in almost the same way in particle and fluid models. The electron and positive ion densities are given by a Gaussian distribution:

$$n_i(\mathbf{r}) = n_e(\mathbf{r}) = 10^{16} \, \text{m}^{-3} \exp \left[\frac{(\mathbf{r} - \mathbf{r_0})^2}{(0.1 \, \text{mm})^2} \right], \qquad (7)$$

where $\mathbf{r_0}$ is the location of the tip of the electrode, which is at $z \approx 7.8 \, \text{mm}$.

In particle simulations, these initial densities are converted to $N = \lfloor n_e \Delta V \rfloor$ simulation particles per cell,
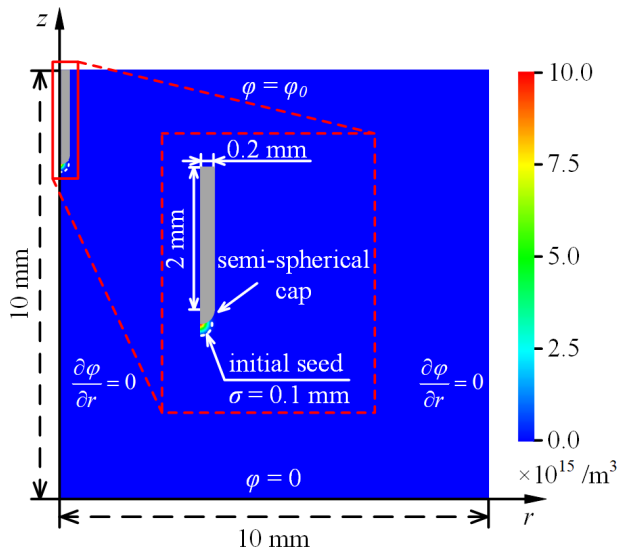
Figure 2: Schematic view of the axisymmetric computational domain used for both particle and fluid models, showing the initial electron density and the electrode. 3D simulations are performed in a similarly sized domain, measuring 20 mm × 20 mm × 10 mm.

each with a weight of one. A uniform $[0, 1)$ random number is compared to the remainder to determine whether to add one more particle. The goal of this sampling is to reduce stochastic fluctuations in the initial conditions. The initial particles are spread uniformly within each grid cell, and they initially have zero kinetic energy.

2.4. Photoionization

For streamers in air, photoionization is typically the main source of free electrons. The process results from the interaction between an oxygen molecule and an UV photon emitted from an excited nitrogen molecule. We use Zheleznyak's model for photoionization in air [50] and compute photoionization as in [17]. Assuming that ionizing photons do not scatter and their direction is isotropically distributed, the photoionization source term in equation (6) is given by:

$$S_{ph}(\mathbf{r}) = \int \frac{I(r')f(|\mathbf{r} - \mathbf{r}'|)}{4\pi \, |\mathbf{r} - \mathbf{r}'|^2} d^3 r', \qquad (8)$$

where $f(r)$ is the photon absorption function and $I(\mathbf{r})$ is the source of ionizing photons, which is proportional to the electron impact ionization source term S_i:

$$I(\mathbf{r}) = \frac{p_q}{p + p_q} \xi S_i, \qquad (9)$$

where p is the gas pressure, $p_q = 40$ mbar is a quenching pressure. For simplicity, we use a constant proportionality factor $\xi = 0.075$, except for section 3.4, in which ξ is varied.

We solve equation (8) in two ways in this paper. For fluid simulations, we use the so-called Helmholtz expansion [51, 52]. By approximating the absorption function, the integral in equation (8) can be turned into multiple Helmholtz equations that can be solved by fast elliptic solvers. We use Bourdon's three-term expansion, as described in [51] and appendix A of [32].

For particle simulations, we use a discrete Monte Carlo photoionization model as described in [17, 53]. With this model stochastic effects due to discrete single photons are simulated. The basic idea is to stochastically sample the generated photons, their directions, and their travel distances. We also use this approach for the fluid simulations in section 3.4, see [17] and chapter 11 of [54] for details.

These two approaches for photoionization differ not only in terms of stochastic effects. Because of the way the absorption function is approximated in the Helmholtz approach, the number of ionizing photons produced and their absorption profile will also be somewhat different. However, such small differences in photoionization usually have only a minor effect on discharge development, as confirmed by our results in section 3.

2.5. Afivo AMR framework

The open-source Afivo framework [37] is used in both particle and fluid models to provide adaptive mesh refinement (AMR) and a parallel multigrid solver. Adaptive mesh refinement (AMR) is used for computational efficiency, based on the following criteria [15]:

- refine if $\alpha(E)\Delta x > c_0$,
- de-refine if $\alpha(E)\Delta x < 0.125c_0$, but only if Δx is smaller than 10 μm.

Here Δx is the grid spacing, which is equal in all directions, $\alpha(E)$ is the field-dependent ionization coefficient, and c_0 is a constant. Furthermore, the grid spacing is bound by $\Delta x \leq 0.4$ mm. For 3D particle simulations we use $c_0 = 1.0$ and for all other simulations $c_0 = 0.8$. Slightly less refinement is used for the 3D particle simulations because of their large computational cost, see Appendix A. With these values for c_0 numerical convergence errors are reasonably small, as discussed in section 3.3.

The geometric multigrid solver in Afivo [37] is used to efficiently solve Poisson's equation $\nabla^2 \phi = \rho/\varepsilon_0$, where ϕ is the electric potential, ε_0 the permittivity of vacuum and ρ the space charge density. Electrostatic fields are then computed as $\vec{E} = -\nabla\phi$. The same type of multigrid solver is also used to solve the Helmholtz equations for photoionization. To include a needle electrode, we set the applied potential as a boundary condition at the electrode surface. This

Model	Data	z (3 ns)	z (6 ns)	z (9 ns)
PIC-2D	-	6.45	4.74	2.41
PIC-3D	-	6.45	4.71	2.39
fluid-2D	flux	6.40	4.64	2.31
fluid-3D	flux	6.42	4.66	2.35
fluid-2D	B+ temp.	6.42	4.71	2.47
fluid-2D	B+ spat.	6.72	5.46	3.87
fluid-2D	bulk-a	6.19	4.13	1.34
fluid-2D	bulk-b	6.54	5.04	3.12

Table 1: Streamer head position (z, in mm) at 3, 6 and 9 ns in different simulations, using an applied voltage of 11.7 kV. The bottom part of the table gives results for different types of transport data, see section 3.2. Here "B+ (temp.)" and "B+ (spat.)" respectively refer to flux data computed with BOLSIG+ using temporal growth and spatial growth models, and "bulk(a)" and "bulk(b)" refer to two types of bulk coefficients.

was implemented by modifying the multigrid methods using a level-set function.

3. Results

3.1. Axisymmetric and 3D results

In this section, we compare axisymmetric and 3D particle and fluid models, using the computational configuration and initial condition described in section 2.3. A voltage of $\phi = 11.70$ kV is applied, which results in a background field of around 15 kV/cm; about half the breakdown field of air.

Photoionization in the fluid model is here computed with the Helmholtz approximation, whereas the particle model uses a Monte Carlo scheme with discrete photons. To account for stochastic fluctuations, ten runs of the 2D cylindrical and 3D particle models are performed, of which five are shown. For the fluid simulations flux transport data from Monte Carlo swarms is used, see section 2.2.2.

Figure 3 shows the electron densities and electric fields for the different models at $t = 10$ ns. The electric field and electron density profiles are similar for all cases, and the streamer head positions are in good agreement, with deviations in streamer length below 5%. Streamer head positions in all models at $t = 3, 6, 9$ ns are given in table 1.

With the axisymmetric particle model stochastic fluctuations are visible in the streamer radius and the electron densities. As discussed in section 3.4 this is mainly due to the stochastic photoionization used in the particle simulations. Streamers appear to propagate somewhat slower due to these fluctuations. In 3D similar fluctuations are present, but the streamers can now move slightly off axis. The 3D particle

model can in principle capture realistic stochastic fluctuations, but only if single electrons are used instead of super-particles. This is computationally not feasible for the simulations performed here.

Stochastic fluctuations are not present in the fluid simulations, in which the electron densities and electric fields evolve smoothly in time. The results of the cylindrical and 3D fluid models are nearly identical. Small differences can occur because the computational domains correspond to a rectangle and a cylinder, which means that the applied boundary conditions are not equivalent. Furthermore, the numerical grids and operators are also slightly different in these two geometries.

To more quantitatively analyze the differences between models, the maximal field E_{max}, the streamer head position z and streamer velocity v are shown in figure 4. The streamer head position is defined as the z-coordinate where the electric field is maximal. The velocity is shown versus streamer position, otherwise initial differences grow larger over time even if models agree well later on. The streamer velocity is computed as the numerical derivative of the streamer head position, which amplifies fluctuations. We use a second order Savitzky–Golay filter of width five to compute a smoothed velocity from the position versus time data. For the stochastic particle simulations the average of ten runs is shown.

The maximal electric field follows a similar trend in all models, with first a field of about 180 kV/cm and then a relaxation towards a field of about 130–135 kV/cm as the streamers propagate across the gap. When the streamers approach the grounded electrode the maximal field increases again, because the available voltage difference is compressed in a small region.

The peak electric fields during inception differ somewhat, with the particle model having the highest peak at about 190 kV/cm whereas it is about 180 kV/cm for both fluid models. The relaxation of this peak electric field occurs about 0.4 ns earlier in the fluid model. The main reason for this is that near the electrode, the degree of ionization in the streamer channel is somewhat higher in the particle simulations, which initially leads to stronger field enhancement.

For this study, we have designed the initial conditions such that inception behavior would be similar in the particle and fluid simulations, by using a sharp electrode and a compact initial seed with sufficiently many electrons. If we define inception as the moment at which the streamer crosses the position $z = 7.6$ mm, then inception is about 0.04 ns faster in the fluid simulations. This is illustrated in figure 5, which shows the electron density at 0.4 ns and 0.8 ns for the 2D fluid and particle simulations. The difference in streamer position at these times is primarily caused
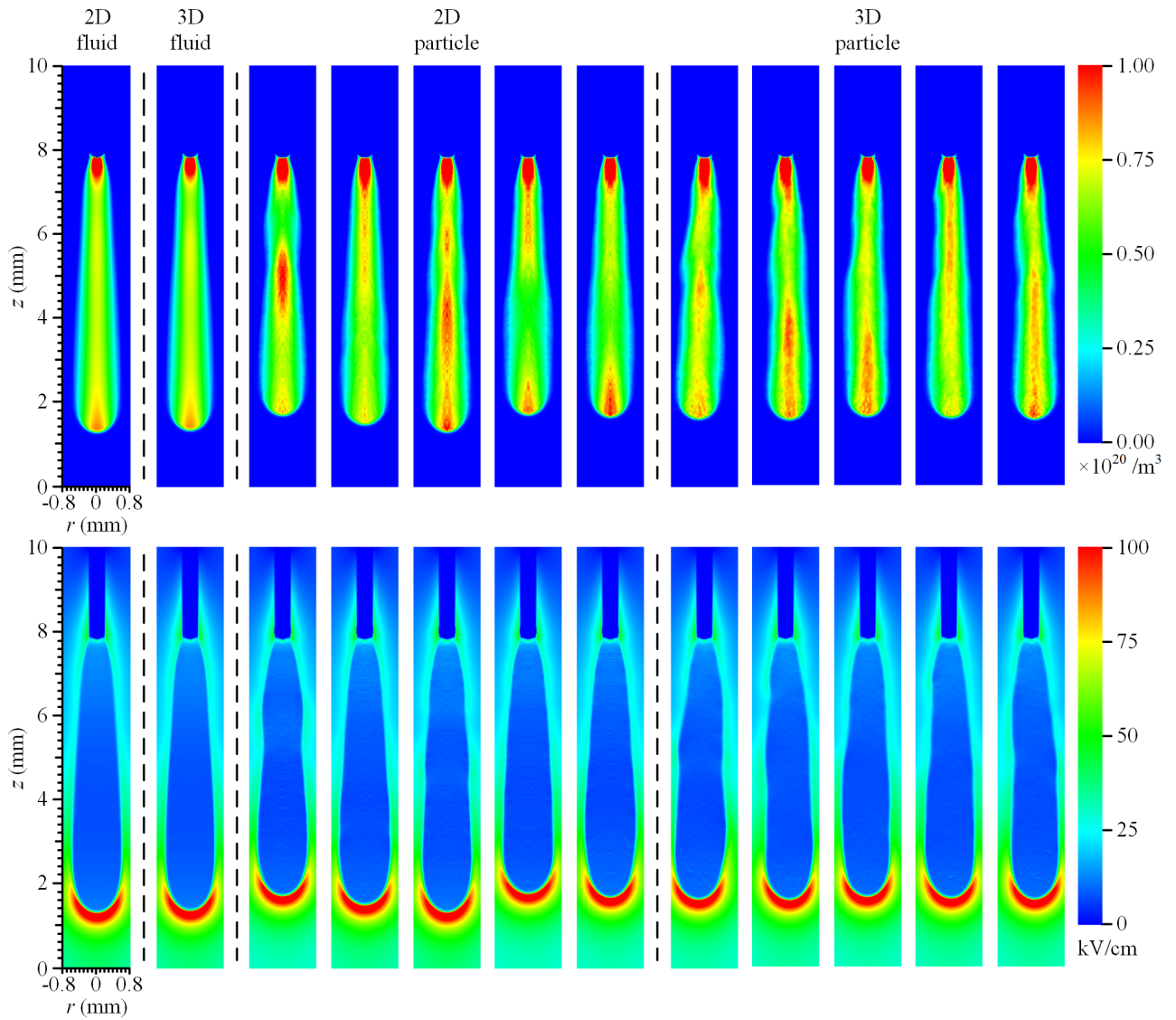
Figure 3: The electron densities and electric fields at $t = 10$ ns for fluid and particle models at an applied voltage of 11.70 kV. The axisymmetric results are mirrored in the symmetry axis. For the 3D simulations cross sections are shown. Multiple runs are shown for the stochastic particle simulations. For the fluid simulations Monte Carlo flux transport data was used.

by faster inception in the fluid model. The difference increases somewhat in time, because a longer streamer propagates faster. Note that the electron density is higher in the particle model.

Faster inception in the fluid model could be due to the local field approximation, with which electrons are assumed to instantaneously relax to the background electric field. Electron multiplication therefore happens more rapidly in the fluid simulations at $t = 0$ ns, and similarly photoelectrons also instantaneously produce new ionization. We remark that when inception is highly stochastic (with different initial conditions), another difference could be more

relevant. With a fluid model low densities always rapidly grow in a high field, even if they correspond to a small probability of an electron being present, as was observed in [55]. Such continuous growth of a low electron density in high field regions can then lead to faster inception.

There is good agreement among the models for the streamer position versus time, and thus also for the streamer velocities as a function of streamer position. Velocity differences are generally less than 0.04 mm/ns among the models. The mean relative deviation in
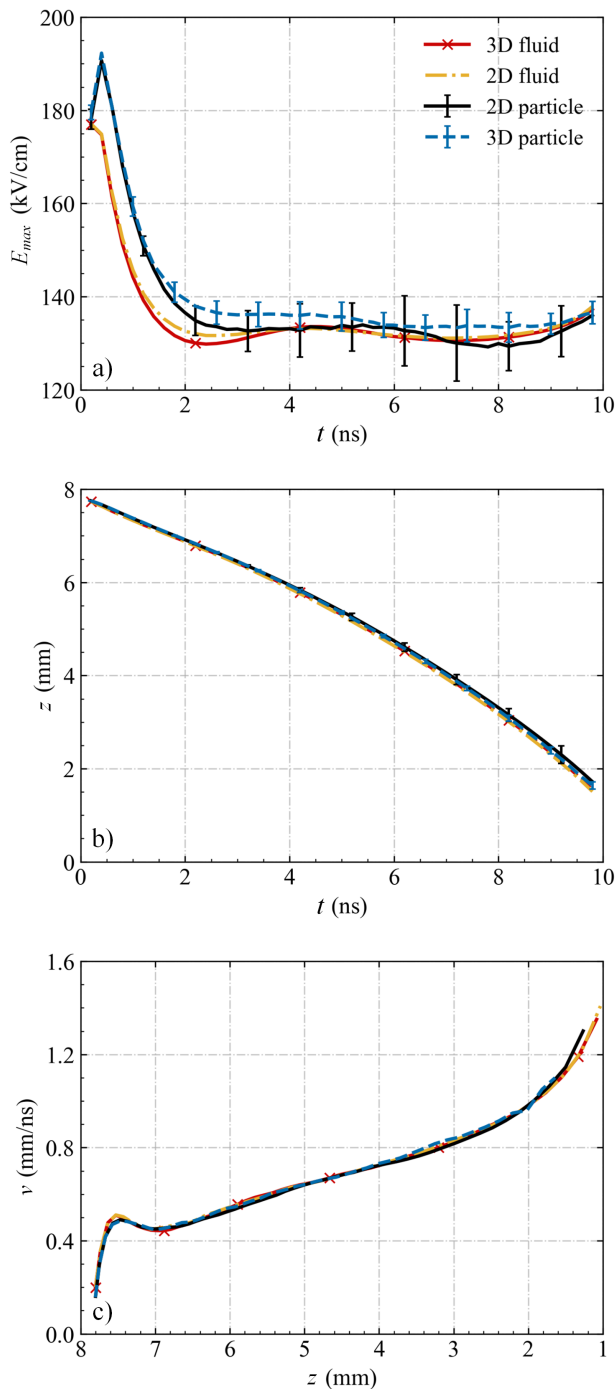
Figure 4: Comparison between axisymmetric and 3D particle and fluid simulations at an applied voltage of 11.70 kV. From top to bottom: maximal electric field versus time, streamer head position versus time and front velocity versus streamer position. For the stochastic particle simulations the average of ten runs is shown, and the error bars indicate $\pm$ one standard deviation.
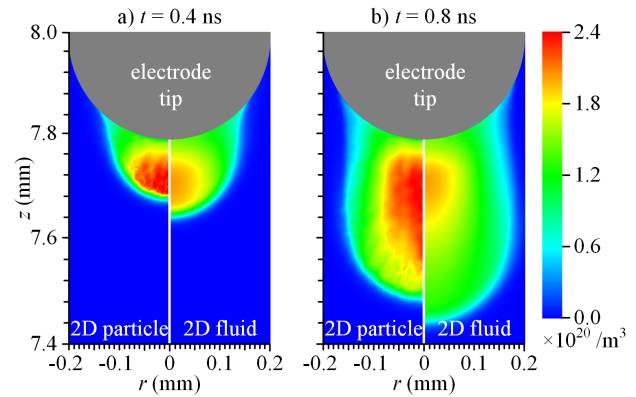

Figure 5: Electron density at 0.4 ns and 0.8 ns in the axisymmetric particle and fluid simulations, for an applied voltage of 11.70 kV. Results from one representative particle simulation are shown; stochastic fluctuations are initially small with the initial conditions used here.

velocity is below 2%. We compute this quantity as

$$\int |v_a(z) - v_b(z)| dz \Big/ \int v_a(z) dz \ , \tag{10}$$

where v_a and v_b denote the velocities in the particle and fluid simulations, which are linearly interpolated between known positions. After inception velocities increase approximately linearly with streamer length. At the end of the gap they increase more rapidly due to boundary effects.

Figure 6 shows the streamer radius versus position in axisymmetric particle and fluid simulations. Good agreement is found between the models, with the maximal difference in radius being below 0.02 mm. Note that there are substantial fluctuations in the radius in the particle simulations as indicated by the error bars. For 3D simulations the radius is harder to compute, as it depends on the viewing angle. However, as can be seen from figure 3, the radius appears to in good agreement between the 2D and 3D simulations.

3.2. Fluid model transport and reaction data

As mentioned in section 2.2.2, transport and reaction data for a fluid model can be computed using different types of Boltzmann solvers. Furthermore, both so-called *flux* and *bulk* data can be computed. Flux data describes the behavior of individual electrons, whereas bulk data describes the behavior of a group of electrons, taking ionization and attachment into account. We here study how the choice of fluid model input data affects the the consistency between particle and fluid simulations. The following types of input data are considered (with labels in bold):
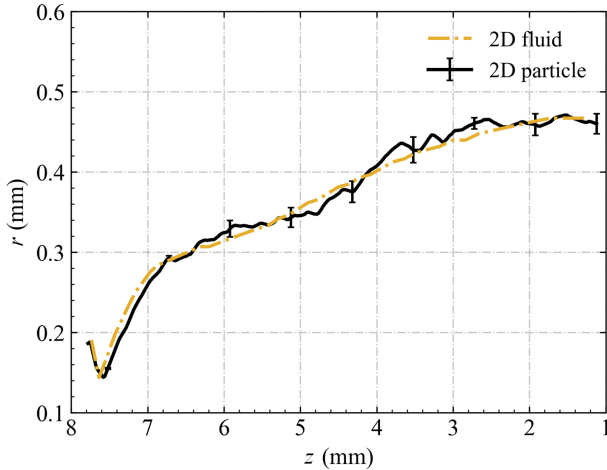
Figure 6: Streamer radius versus position for axisymmetric particle and fluid simulations at an applied voltage of 11.70 kV. The streamer radius was here defined as the radius at which E_r, the radial component of the electric field, is maximal. For the stochastic particle simulations the average of ten runs is shown, and the error bars indicate $\pm$ one standard deviation.

- (**B+ temp.**) Flux data computed with BOLSIG+ using its temporal growth model [30]. With this setting, the two-term approximation is solved by assuming that the electron density grows exponentially in time. This is the default growth model, but it is not clear whether it is the most suitable growth model for streamer simulations [30].

- (**B+ spat.**) Flux data computed with BOLSIG+ using its spatial growth model [30], in which it is assumed that the electron density grows exponentially in space.

- (**flux**) Flux data computed with a Monte Carlo swarm method (available at `gitlab.com/MD-CWI-NL/particle_swarm`), which uses the same core routines for simulating electrons as our particle model [10].

- (**bulk-a**) Bulk data computed with the same Monte Carlo swarm method. In this variant, only the transport terms in equation (6) are modified, by computing the electron flux as $-n_e \mu_e^B \mathbf{E} - D_e^B \nabla n_e$, where μ_e^B and D_e^B denote bulk coefficients.

- (**bulk-b**) The same bulk data as above, but in this variant the reaction terms in equation (6) are also modified by multiplying them with μ_e^B / μ_e, where μ_e denotes the standard flux mobility.

With the **bulk-a** approach reaction rates are the same as with flux data. However, the number of reactions taking place per unit length (traveled by electrons) is changed, i.e., the so-called Townsend coefficients are different. With the **bulk-b** approach it is the other way around.

Different types of transport data are shown in figure 7. Above about 180 Td ionization becomes important and bulk mobilities are larger than flux mobilities. The spatial growth model of BOLSIG+ leads to a significantly smaller ionization coefficient. In high electric fields, its value is about 25-30% less than that of the other approaches. With the Monte Carlo approach both transverse and longitudinal diffusion coefficients are computed, but in our fluid simulations we for simplicity only use the transverse ones. The BOLSIG+ flux diffusion coefficient also corresponds to the transverse direction [30, 44], but it is larger than the Monte Carlo flux coefficient. Such differences between diffusion coefficients computed with a two-term approach and higher-order methods have been observed before, see e.g. [27]. However, the different diffusion coefficients only have a minor impact on our simulations, as shown below.

Figure 8 shows axisymmetric fluid simulations with the input data listed above; streamer positions over time are given in table 1 and streamer velocities in figure 9. There are minor differences in streamer velocity when comparing the BOLSIG+ flux data with temporal growth and the Monte Carlo flux data. When comparing streamer velocities at the same length, relative differences are below 3%. With both types of data good agreement is obtained with the axisymmetric particle simulations. In contrast, the BOLSIG+ data with the spatial growth model leads to a streamer velocity that is much too low, due to the lower ionization coefficient.

Both types of bulk transport data lead to significant deviations compared to the particle model. When only the transport coefficients are changed (bulk-a), the streamer is significantly slower and it has a lower degree of ionization. With this data electrons drift faster, but the degree of ionization produced in the streamer channel is lower, leading to a slower discharge. However, when the reaction terms are also changed (bulk-b), the streamer propagates too fast. The higher streamer velocity is to be expected, since most terms on the right-hand side of equation (6) are now scaled with the bulk mobility.

In conclusion, bulk data and data computed with a spatial growth model are not recommended for the simulation of positive streamers. With flux transport data there are minor differences between BOLSIG+ data computed with a temporal growth model and Monte Carlo data, but both lead to good agreement with the particle simulations.
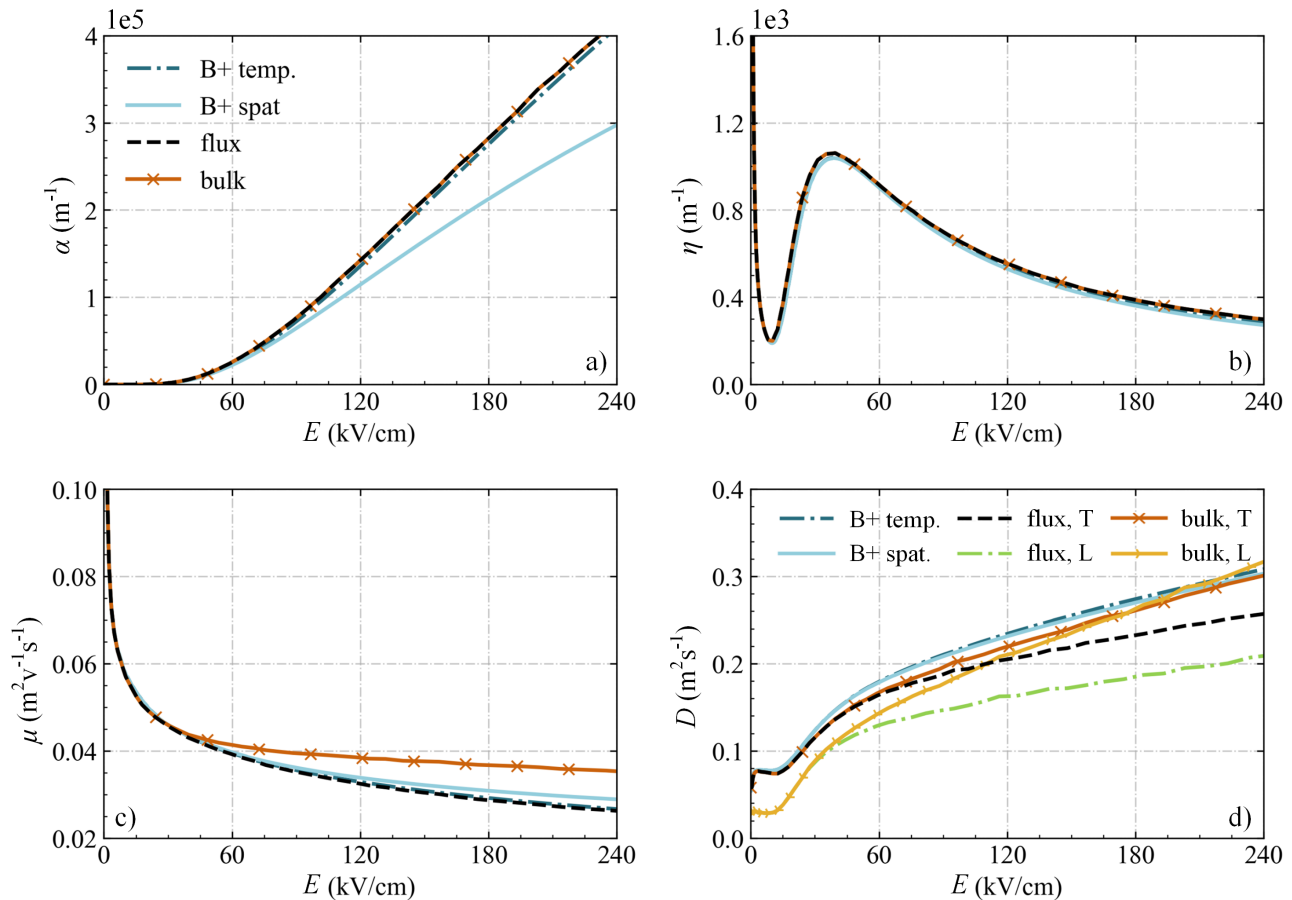
Figure 7: Electron transport data. a) Ionization coefficient, b) attachment coefficient, c) electron mobility and d) electron diffusion coefficient. The coefficients were computed for 80% N_2 and 20% O_2 at 1 bar and 300 K, using Phelp's cross sections, see section 2.1.5. For BOLSIG+, data is shown using both a temporal and a spatial growth model. The data labeled "bulk" and "flux" was computed with a Monte Carlo swarm code. Both transverse and longitudinal diffusion coefficients were computed with this technique, but only the transverse coefficients are used in our fluid model.

3.3. Mesh refinement and numerical convergence

We here study the sensitivity of the particle and fluid simulations to the grid spacing, to test whether our simulations are close to numerical convergence. To control the grid spacing, the refinement parameter c_0 is varied, see section 2.5. Note that the time step in both models will also be affected by the grid spacing, as explained in section 2.1.4 and 2.2.1.

Figure 10 shows streamer velocities versus streamer position for c_0 values of 1.0, 0.8, 0.4 and 0.2, for which the minimal grid spacing is 3.9, 3.9, 1.9, and 0.9 μm, respectively. Streamer positions at $t = 3$, 6 and 9 ns are given in table 2. With the fluid model, deviations in length at $t = 9$ ns are about 3% with $c_0 = 0.8$ compared to the finest-grid case. With the particle model, there are statistical fluctuations that make it harder to establish numerical convergence, but at $t = 9$ ns streamer lengths are also within 3% for all

tested cases. When comparing the streamer velocity versus position for $c_0 = 0.8$ and $c_0 = 0.2$, convergence errors are about 1% for the fluid model and about 2% for the particle model, using equation (10).

Table 2 allows to compare differences in streamer length between particle and fluid simulations using the same refinement. Interestingly, these differences are larger on finer grids: with $c_0 = 0.2$, the relative differences in streamer length are about 8–10% at 3, 6 and 9 ns, whereas for $c_0 = 0.8$ they are about 2–4%. For streamer velocities (compared at the same streamer length) the mean deviations are about 4% and 2% for these two cases, using equation (10).

Based on the above, we conclude that numerical convergence errors are relatively small for our default refinement parameter $c_0 = 0.8$ – they do at least not exceed the intrinsic differences between the models, which are already quite small. For the test case

a) electron density
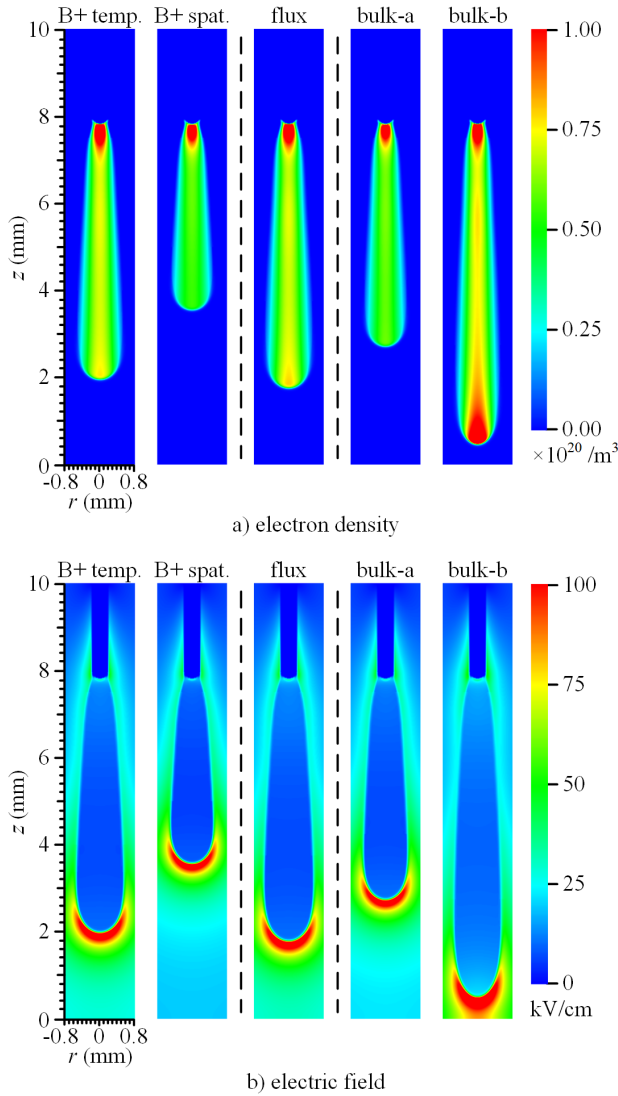
b) electric field

Figure 8: Electron densities and electric fields at $t = 9.6$ ns for axisymmetric fluid simulations with an applied voltage of 11.7 kV. Different types of transport data are used, from left to right: BOLSIG+ with temporal growth, BOLSIG+ with spatial growth, Monte Carlo flux data, and two types of Monte Carlo bulk data. With bulk-a only transport terms are modified, and with bulk-b reaction terms are also scaled with the bulk mobility.
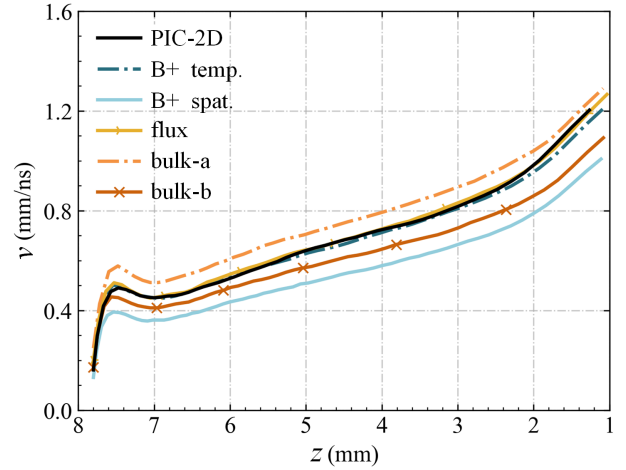

Figure 9: Streamer velocity versus streamer head position for different types of transport data. The labels are explained in figure 8 and in section 3.2.
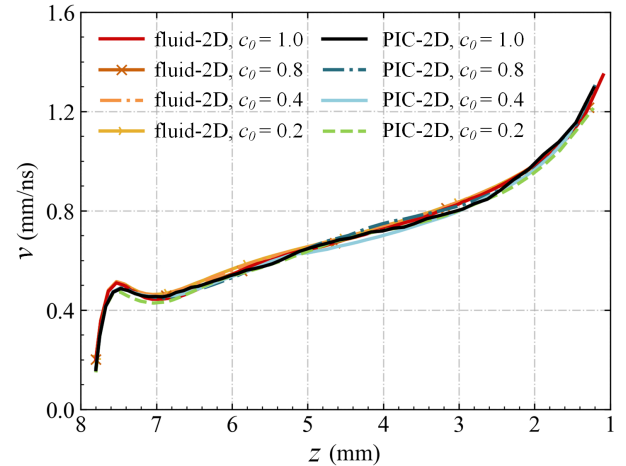

Figure 10: Streamer front velocities versus streamer head position for different refinement criteria. Other conditions are the same as in section 3.1. For the particle simulations the average of ten runs is shown to reduce stochastic fluctuations.

considered here, with an applied voltage of 11.7 kV, the difference in streamer velocity is about twice as large (4% instead of 2%) on the finest grid. The main reason for this is that in the fluid simulations, which are more sensitive to the grid refinement, the streamer velocity is somewhat higher on finer grids. In section 3.5 we show that for higher applied voltages, the velocity is actually higher in the particle simulations. We therefore expect that using a finer grid somewhat increases model discrepancies for lower applied voltages, and that is somewhat reduces model discrepancies for higher applied voltages.

Model	c_0	z (3 ns)	z (6 ns)	z (9 ns)
PIC-2D	0.2	6.51	4.81	2.59
		± 0.02	± 0.09	± 0.11
PIC-2D	0.4	6.45	4.74	2.54
		± 0.03	± 0.04	± 0.06
PIC-2D	0.8	6.45	4.74	2.41
		± 0.03	± 0.11	± 0.21
PIC-2D	1.0	6.45	4.71	2.45
		± 0.04	± 0.13	± 0.13
fluid-2D	0.2	6.37	4.54	2.14
fluid-2D	0.4	6.37	4.55	2.17
fluid-2D	0.8	6.40	4.64	2.31
fluid-2D	1.0	6.42	4.67	2.35

Table 2: Streamer head position (z, in mm) at 3, 6 and 9 ns, using an applied voltage of 11.7 kV. Different values of the refinement parameter c_0 are used, see section 2.5. For the particle simulations averages over ten runs are shown, together with the standard deviation of the sample. Streamer lengths are given by $7.8\,\mathrm{mm} - z$.

3.4. Stochastic fluctuations

To investigate the source of stochastic fluctuations in the axisymmetric simulations we vary two parameters. The first is the photoionization factor ξ, see equation 9, which is a proportionality factor that relates the number of UV photons produced to the electron impact ionization source term. It therefore directly controls the amount of photoionization. To study how ξ affects stochastic behavior, we use the discrete photoionization model in both the particle and the fluid simulations presented here. The second parameter we vary is N_{ppc}, which controls the 'desired' number of particles per cell in particle simulations, see equation 3.

Figure 11 shows results of axisymmetric particle and fluid models for $\xi = 0.0375$, 0.075, 0.15 and N_{ppc} = 50, 100, 200. In both models the streamer length is not sensitive to the amount of photoionization, as was also observed in e.g. [56]. However, fluctuations in the electron density are significantly larger for the ξ = 0.0375 case, whereas these fluctuations are reduced for the ξ = 0.15 case, as was also observed in [17]. With ξ = 0.0375 we even observed branching in a few of the simulation runs, which is probably due to increased density fluctuations near the z-axis when the amount of photoionization is decreased. Fluctuations in the streamer radius are also larger for a lower value of ξ. When N_{ppc} is increased, fluctuations in electron densities and streamer radius are slightly reduced, but the effect is weaker than that of the ξ parameter. We therefore conclude that the discrete photoionization model is responsible for most of the

stochastic fluctuations in our results. This confirms the assumptions made in recent work [17,57], in which fluid models were used to demonstrate the importance of stochastic photoionization on streamer branching.

Finally, we remark that in figure 11 the stochastic fluctuations are demonstrated with axisymmetric models, in which these fluctuations are not completely physical. We have also performed 3D fluid simulations with stochastic photoionization, in which these fluctuations looked qualitatively similar to those shown in figure 3 for the 3D particle model. However, a statistical comparison of these 3D models for the parameter range shown in figure 11 could not be performed due to the high computational costs of the 3D particle simulations.

3.5. Results at different voltages

Figure 12 shows results for particle and fluid simulations at a higher applied voltage of 14.04 kV, which results in a background electric field of about 18 kV/cm. All the other parameters are the same as in section 3.1. For the 3D particle model results at later times are missing, because these simulations exceeded the memory and time constraints of our computational hardware, see Appendix A.

At this higher voltage, the agreement between the models is of similar quality as in figure 4, but there are a few differences. Figure 12(a) shows that inception is significantly faster. The relaxation of the initial high field takes place in about 1 ns, so roughly twice as fast, and the curves for the maximal electric field are now in better agreement. With a higher applied voltage the streamer velocity is higher, but the propagation is otherwise similar to that in figure 4. The agreement between the models is still good: between the 2D particle and 2D fluid simulations, the mean deviation in velocity (compared at the same streamer length) is about 1%. However, the discrepancy between the 2D and 3D fluid simulations is now somewhat larger. This is probably due to the difference in computational domains and electrostatic boundary conditions in 2D and 3D, which could play a stronger role for a more conducting streamer channel at a higher voltage. The sensitivity of discharge simulations to these boundary conditions was recently observed in [55].

Figure 13 shows the relative difference Δ_L in streamer length between axisymmetric particle and fluid models for applied voltages from 11.70 kV to 15.60 kV. These voltages correspond to background electric fields of about 15 kV/cm to 20 kV/cm. The difference is computed as

$$\Delta_L = (L_{\mathrm{fluid,2D}} - L_{\mathrm{pic,2D}})/L_{\mathrm{pic,2D}},$$

where $L_{\mathrm{fluid,2D}}$ and $L_{\mathrm{pic,2D}}$ are the streamer lengths in the fluid and particle model at a particular time.
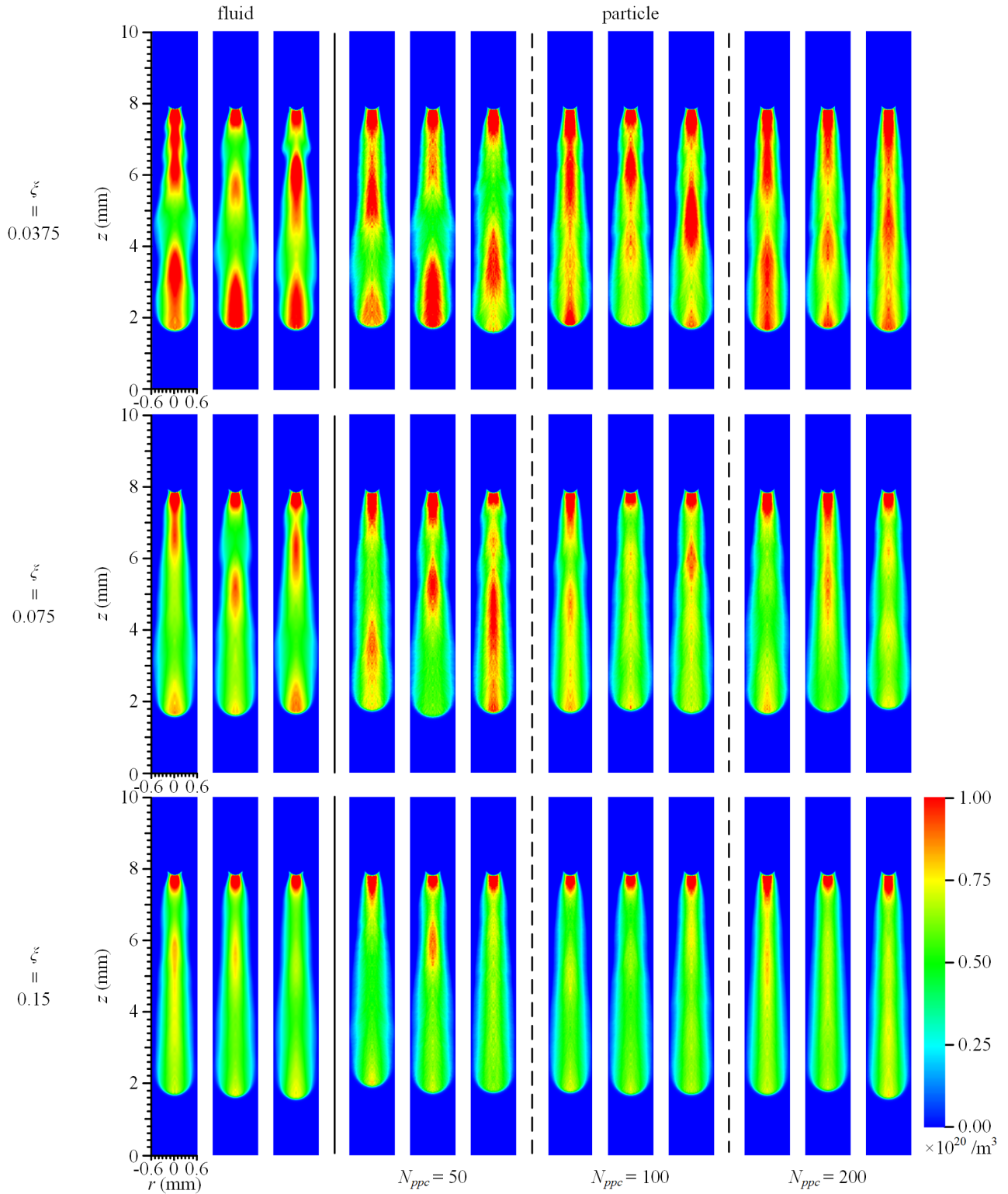
Figure 11: Electron densities at $t = 10$ ns in axisymmetric fluid and particle simulations. The photoionization coefficient ξ and the desired number of particles per cell N_{ppc} are varied. For each combination of two parameters, three runs are shown. Stochastic photoionization is now also used in the fluid model. The condition are otherwise the same as in section 3.1.
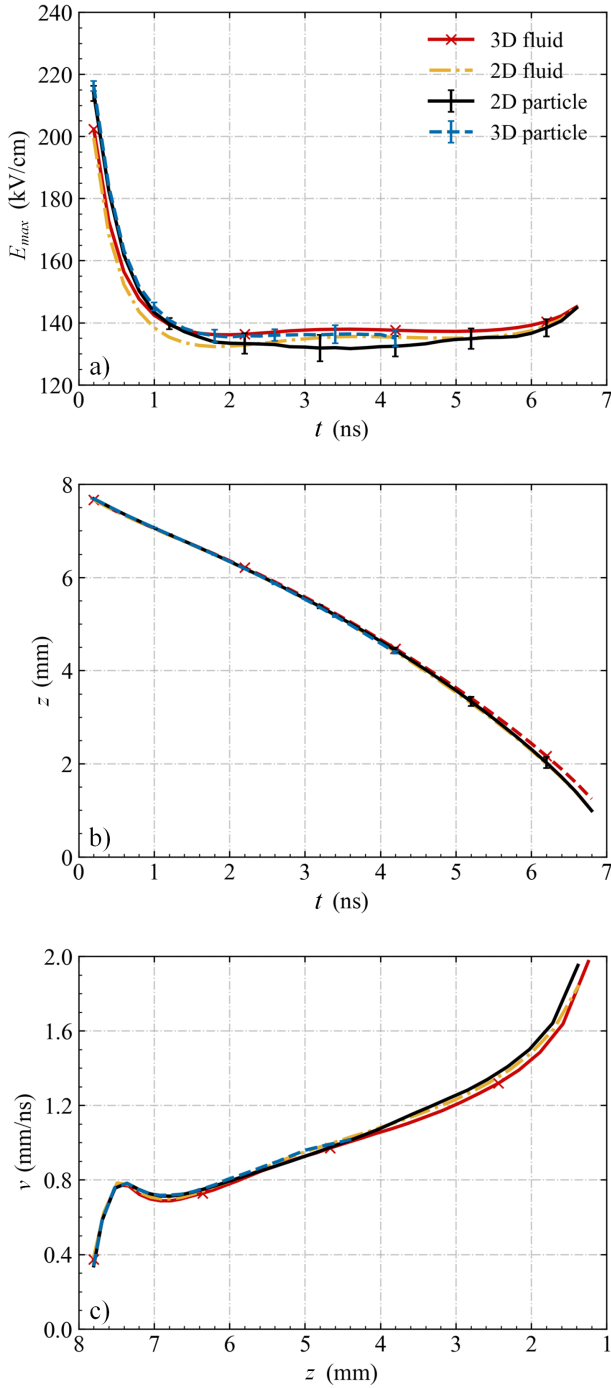
Figure 12: Comparison between axisymmetric and 3D particle and fluid models at an applied voltage of 14.04 kV, similar to figure 4. From top to bottom: the maximal electric field and streamer position versus time, and streamer velocity versus streamer position. For the particle model the average of ten runs is shown with error bars indicating $\pm$ one standard derivation.
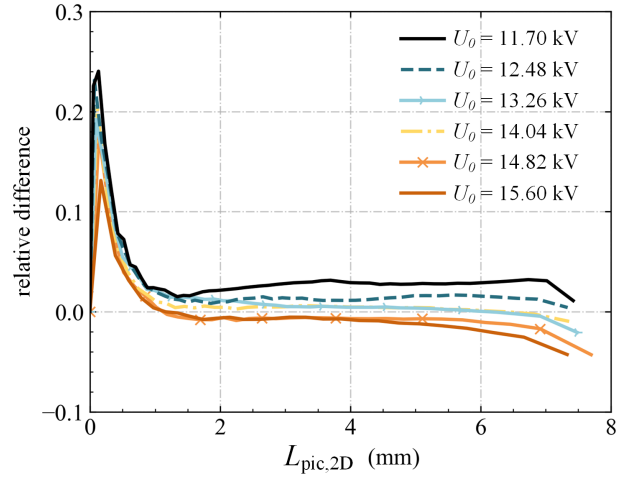

Figure 13: The relative difference Δ_L in streamer length versus time, shown for axisymmetric particle and fluid simulations at several voltages. The difference is computed as $\Delta_L = (L_{\text{fluid,2D}} - L_{\text{pic,2D}})/L_{\text{pic,2D}}$. Besides the applied voltage, simulations conditions are the same as in section 3.1.

In all cases, Δ_L peaks during streamer inception. This happens because inception occurs faster in the fluid model, as explained in section 3.1, and because the denominator is initially small. For higher applied voltages, the initial peak in Δ_L becomes smaller.

In which model the streamer has advanced the furthest at a particular time depends on the applied voltage. When U_0 is lower than 14.04 kV, Δ_L is generally positive, whereas for higher voltages it becomes negative. This indicates that relative to the fluid simulations, the velocity in the particle simulations is higher at higher voltages. The mean deviations between velocities in the particle and fluid simulations are 1.8% (11.7 kV case), 1.9% (12.48 kV), 1.3% (13.26 kV), 1.3% (14.04 kV), 1.4% (14.82 kV) and 2.4% (15.6 kV).

4. Conclusions

We have quantitatively compared a PIC-MCC (particle-in-cell, Monte Carlo collision) model and a drift-diffusion-reaction fluid model with the local field approximation for simulating positive streamer discharges. The simulations were performed in air at 1 bar and 300 K, in background fields below breakdown ranging from 15 kV/cm to 20 kV/cm, using both axisymmetric and fully three-dimensional geometries.

We have found surprisingly good agreement between the particle and fluid simulations. Streamer properties such as maximal field, radius, and velocity were all very similar. When compared at the same

streamer length, the mean difference in streamer velocity was generally below 4%. One source of differences was the photoionization model, for which we used a stochastic approach in the particle simulations and a continuum approach in most of the fluid simulations.

We have investigated the effect of different types of transport data in fluid models, how well the models are numerically converged, what the main source of stochastic fluctuations is, and how the agreement between the models is affected by the applied voltage. Our main conclusions on these topics are:

- The type of transport data used in a fluid model is important. By using flux transport coefficients computed with a Monte Carlo approach or BOLSIG+ (using its temporal growth model), good agreement is obtained between the fluid and particle simulations. The use of bulk coefficients leads to either faster or slower streamer propagation, depending on how the coefficients are used. Data computed with the spatial growth model of BOLSIG+ leads to a significantly slower streamer discharge.

- Numerical convergence errors are small in the particle and fluid simulations presented here. We have compared axisymmetric particle and fluid simulations with grid refinement satisfying $\alpha(E)\Delta x < c_0$ for $c_0 = 0.2, 0.4, 0.8$ and 1.0, where $\alpha(E)$ is the ionization coefficient. For an applied voltage of 11.7 kV, convergence errors in streamer velocity (compared at the same position) were about 1% for the fluid simulations and about 2% for the particle simulations. On the finest grids, streamer velocities increased slightly in the fluid simulations.

- Stochastic fluctuations are visible in axisymmetric and 3D particle simulations, for example in the streamer's degree of ionization, maximal electric field and radius. In our simulations, the dominant source of these stochastic fluctuations is discrete photoionization. Fluid simulations with the same discrete photoionization model exhibit similar fluctuations as particle simulations. Due to these fluctuations, streamers in 3D simulations propagate slightly off-axis. In the particle simulations, the number of particles per cell did not significantly affect these fluctuations.

- Axisymmetric simulations were performed for applied voltages between 11.7 kV to 15.6 kV, corresponding to background fields of about 15 kV/cm to 20 kV/cm. Discrepancies in streamer length (versus time) between particle and fluid simulations were generally below 3%. The mean deviations in streamer velocity (versus length) were about 2% for all applied voltages. Other

streamer properties, such as the maximal electric field, were also in good agreement.

Finally, we expect differences between particle and fluid models to increase at lower applied electric fields. Inception will be more stochastic, and a smaller streamer radius in lower fields will lead to steeper gradients in the electron density and electric field, which could increase errors due to the local field approximation. However, a comparison in lower fields, in which streamer branching would probably have to be taken into account, is left for future work.

Acknowledgments

Data availability statement

The data that support the findings of this study are openly available at the following URL/DOI: `https://doi.org/10.5281/zenodo.5509678`.

Appendix A. Computational cost

Typical computing times for the results in section 3.1 were a few minutes (2D fluid model), 8h (3D fluid model), and 2-3h (2D particle model). These computations ran on an Intel(R) Core(TM) i9-9900K eight-core processor, using OpenMP parallelization. The 3D particle simulations were performed on Cartesius, the Dutch national supercomputer. A single thin node with a Intel Xeon E5-2690 v3 (Haswell) 24-core processor and 64 GB of RAM was used. Computations ran for up to five days, with up to 600 million particles.

The maximum number of grid cells used for the simulations presented in section 3.1 were: 4.2×10^4 (2D fluid), 1.4×10^8 (3D fluid), 5.1×10^4 (2D particle), 8.3×10^7 (3D particle). For the numerical convergence tests presented in section 3.3, the maximum number of grid cells at $t = 9$ ns were 2.4×10^5, 8.5×10^4, 3.8×10^4, 3.3×10^4 (2D fluid, $c_0 = 0.2, 0.4, 0.8, 1.0$ respectively) and 2.0×10^5, 8.2×10^4, 4.2×10^4, 3.5×10^4 (2D particle, $c_0 = 0.2, 0.4, 0.8, 1.0$ respectively).

References

.

[1] Sander Nijdam, Jannis Teunissen, and Ute Ebert. The physics of streamer discharge phenomena. *Plasma Sources Science and Technology*, 29(10):103001, 2020.

[2] Ute Ebert, Sander Nijdam, Chao Li, Alejandro Luque, Tanja Briels, and Eddie van Veldhuizen. Review of recent results on streamer discharges and discussion of their relevance for sprites and lightning. *Journal of Geophysical Research: Space Physics*, 115(A7), 2010.

[3] Victor P. Pasko, Jianqi Qin, and Sebastien Celestin. Toward Better Understanding of Sprite Streamers: Initiation, Morphology, and Polarity Asymmetry. *Surveys in Geophysics*, 34(6):797–830, November 2013.

[4] Seiji Kanazawa, Hirokazu Kawano, Satoshi Watanabe, Takashi Furuki, Shuichi Akamine, Ryuta Ichiki, Toshikazu Ohkubo, Marek Kocik, and Jerzy Mizeraczyk. Observation of oh radicals produced by pulsed discharges on the surface of a liquid. *Plasma Sources Science and Technology*, 20(3):034010, 2011.

[5] Hyun-Ha Kim. Nonthermal Plasma Processing for Air-Pollution Control: A Historical Review, Current Issues, and Future Prospects. *Plasma Processes and Polymers*, 1(2):91–110, September 2004.

[6] P J Bruggeman, M J Kushner, B R Locke, J G E Gardeniers, W G Graham, D B Graves, R C H M Hofman-Caris, D Maric, J P Reid, E Ceriani, D Fernandez Rivas, J E Foster, S C Garrick, Y Gorbanev, S Hamaguchi, F Iza, H Jablonowski, E Klimova, J Kolb, F Krcma, P Lukes, Z Machala, I Marinov, D Mariotti, S Mededovic Thagard, D Minakata, E C Neyts, J Pawlat, Z Lj Petrovic, R Pflieger, S Reuter, D C Schram, S Schröter, M Shiraiwa, B Tarabová, P A Tsai, J R R Verlet, T von Woedtke, K R Wilson, K Yasui, and G Zvereva. Plasma–liquid interactions: A review and roadmap. *Plasma Sources Science and Technology*, 25(5):053002, September 2016.

[7] Michael Keidar, Alex Shashurin, Olga Volotskova, Mary Ann Stepp, Priya Srinivasan, Anthony Sandler, and Barry Trink. Cold atmospheric plasma in cancer therapy. *Physics of Plasmas*, 20(5):057101, May 2013.

[8] SM Starikovskaia. Plasma-assisted ignition and combustion: nanosecond discharges and development of kinetic mechanisms. *Journal of Physics D: Applied Physics*, 47(35):353001, 2014.

[9] D. V. Rose, D. R. Welch, R. E. Clark, C. Thoma, W. R. Zimmerman, N. Bruner, P. K. Rambo, and B. W. Atherton. Towards a fully kinetic 3D electromagnetic particle-in-cell model of streamer formation and dynamics in high-pressure electronegative gases. *Physics of Plasmas*, 18(9):093501, September 2011.

[10] Jannis Teunissen and Ute Ebert. 3d pic-mcc simulations of discharge inception around a sharp anode in nitrogen/oxygen mixtures. *Plasma Sources Science and Technology*, 25(4):044005, 2016.

[11] Vladimir Kolobov and Robert Arslanbekov. Electrostatic PIC with adaptive Cartesian mesh. *Journal of Physics: Conference Series*, 719:012020, May 2016.

[12] Dmitry Levko, Michael Pachuilo, and Laxminarayan L Raja. Particle-in-cell modeling of streamer branching in CO $_2$ gas. *Journal of Physics D: Applied Physics*, 50(35):354004, September 2017.

[13] J Stephens, M Abide, A Fierro, and A Neuber. Practical considerations for modeling streamer discharges in air with radiation transport. *Plasma Sources Science and Technology*, 27(7):075007, July 2018.

[14] Natalia Yu Babaeva, Dmitry V Tereshonok, and George V Naidis. Fluid and hybrid modeling of nanosecond surface discharges: Effect of polarity and secondary electrons emission. *Plasma Sources Science and Technology*, 25(4):044008, July 2016.

[15] Jannis Teunissen and Ute Ebert. Simulating streamer discharges in 3d with the parallel adaptive afivo framework. *Journal of Physics D: Applied Physics*, 50(47):474001, 2017.

[16] J-M Plewa, O Eichwald, O Ducasse, P Dessante, C Jacobs, N Renon, and M Yousfi. 3D streamers simulation in a pin to plane configuration using massively parallel computing. *Journal of Physics D: Applied Physics*, 51(9):095206, March 2018.

[17] Behnaz Bagheri and Jannis Teunissen. The effect of the stochasticity of photoionization on 3d streamer simulations. *Plasma Sources Science and Technology*, 28(4):045013, 2019.

[18] Robert Marskar. An adaptive Cartesian embedded boundary approach for fluid simulations of two- and three-dimensional low temperature plasma filaments in complex geometries. *Journal of Computational Physics*, 388:624–654, July 2019.

[19] A Yu Starikovskiy and N L Aleksandrov. How pulse polarity and photoionization control streamer discharge development in long air gaps. *Plasma Sources Science and Technology*, 29(7):075004, July 2020.

[20] Ryo Ono and Atsushi Komuro. Generation of the single-filament pulsed positive streamer discharge in atmospheric-pressure air and its comparison with two-dimensional simulation. *Journal of Physics D: Applied Physics*, 53(3):035202, January 2020.

[21] S Dujko, A H Markosyan, R D White, and U Ebert. High-order fluid model for streamer discharges: I. Derivation of model and transport data. *J. Phys. D: Appl. Phys.*, 46(47):475202, October 2013.

[22] N A Garland, D G Cocks, G J Boyle, S Dujko, and R D White. Unified fluid model analysis and benchmark study for electron transport in gas and liquid analogs. *Plasma Sources Science and Technology*, 26(7):075003, June 2017.

[23] U Kortshagen, C Busch, and L D Tsendin. On simplifying approaches to the solution of the Boltzmann equation in spatially inhomogeneous plasmas. *Plasma Sources Science and Technology*, 5(1):1–17, February 1996.

[24] D Trunec, Z Bonaventura, and D Nečas. Solution of time-dependent Boltzmann equation for electrons in non-thermal plasma. *Journal of Physics D: Applied Physics*, 39(12):2544–2552, June 2006.

[25] P J Drallos, V P Nagorny, and W Williamson. A kinetic study of the local field approximation in simulations of AC plasma display panels. *Plasma Sources Science and Technology*, 4(4):576–590, November 1995.

[26] G. K. Grubert, M. M. Becker, and D. Loffhagen. Why the local-mean-energy approximation should be used in hydrodynamic plasma descriptions instead of the local-field approximation. *Physical Review E*, 80(3):036405, September 2009.

[27] Z Lj Petrović, S Dujko, D Marić, G Malović, Ž Nikitović, O Šašić, J Jovanović, V Stojanović, and M Radmilović-Rađenović. Measurement and interpretation of swarm parameters and their application in plasma modelling. *Journal of Physics D: Applied Physics*, 42(19):194002, October 2009.

[28] RE Robson, Ronald Douglas White, and Z Lj Petrović. Colloquium: Physically based fluid modeling of collisionally dominated low-temperature plasmas. *Reviews of modern physics*, 77(4):1303, 2005.

[29] Chao Li, Jannis Teunissen, Margreet Nool, Willem Hundsdorfer, and Ute Ebert. A comparison of 3d particle, fluid and hybrid simulations for negative streamers. *Plasma Sources Science and Technology*, 21(5):055019, 2012.

[30] GJM Hagelaar and LC Pitchford. Solving the boltzmann equation to obtain electron transport coefficients and rate coefficients for fluid models. *Plasma Sources Science*

and Technology, 14(4):722, 2005.

[31] Aram H Markosyan, Jannis Teunissen, Saša Dujko, and Ute Ebert. Comparing plasma fluid models of different order for 1d streamer ionization fronts. *Plasma Sources Science and Technology*, 24(6):065002, 2015.

[32] Behnaz Bagheri, Jannis Teunissen, Ute Ebert, Markus M Becker, She Chen, Olivier Ducasse, Olivier Eichwald, Detlef Loffhagen, Alejandro Luque, Diana Mihailova, et al. Comparison of six simulation codes for positive streamers in air. *Plasma Sources Science and Technology*, 27(9):095002, 2018.

[33] HC Kim, Felipe Iza, SS Yang, M Radmilović-Radjenović, and JK Lee. Particle and fluid simulations of low-temperature plasma discharges: benchmarks and kinetic effects. *Journal of Physics D: Applied Physics*, 38(19):R283, 2005.

[34] S. H. Lee, F. Iza, and J. K. Lee. Particle-in-cell Monte Carlo and fluid simulations of argon-oxygen plasma: Comparisons with experiments and validations. *Physics of Plasmas*, 13(5):057102, May 2006.

[35] Y J Hong, M Yoon, F Iza, G C Kim, and J K Lee. Comparison of fluid and particle-in-cell simulations on atmospheric pressure helium microdischarges. *Journal of Physics D: Applied Physics*, 41(24):245208, December 2008.

[36] M M Becker, H Kählert, A Sun, M Bonitz, and D Loffhagen. Advanced fluid modeling and PIC/MCC simulations of low-pressure ccrf discharges. *Plasma Sources Science and Technology*, 26(4):044001, April 2017.

[37] Jannis Teunissen and Ute Ebert. Afivo: A framework for quadtree/octree amr with shared-memory parallelization and geometric multigrid methods. *Computer Physics Communications*, 233:156–166, 2018.

[38] Katsuhisa Koura. Null-collision technique in the direct-simulation Monte Carlo method. *Physics of Fluids*, 29(11):3509, 1986.

[39] R. W. Hockney and J. W. Eastwood. *Computer Simulation Using Particles.* IOP Publishing Ltd., Bristol, England, 1988.

[40] Jannis Teunissen and Ute Ebert. Controlling the weights of simulation particles: Adaptive particle management using k-d trees. *Journal of Computational Physics*, 259:318–330, February 2014.

[41] Samuel J. Araki and Richard E. Wirz. Cell-centered particle weighting algorithm for PIC simulations in a non-uniform 2D axisymmetric mesh. *Journal of Computational Physics*, 272:218–226, September 2014.

[42] AV Phelps and LC Pitchford. Anisotropic scattering of electrons by n 2 and its effect on electron transport. *Physical Review A*, 31(5):2932, 1985.

[43] Phelps database (N2,O2). www.lxcat.net, retrieved on March 30, 2021.

[44] L. C. Pitchford and A. V. Phelps. Comparative calculations of electron-swarm properties in N 2 at moderate E N values. *Physical Review A*, 25(1):540–554, January 1982.

[45] B. Koren. A robust upwind discretization method for advection, diffusion and source terms. In C. B. Vreugdenhil and B. Koren, editors, *Numerical Methods for Advection-Diffusion Problems*, pages 117–138. Braunschweig/Wiesbaden: Vieweg, 1993.

[46] Bolsig+ solver. www.lxcat.net, ver. 11/2019.

[47] A Banković, S Dujko, Ronald Douglas White, SJ Buckman, and Z Lj Petrović. On approximations involved in the theory of positron transport in gases in electric and magnetic fields. *The European Physical Journal D*, 66(7):1–10, 2012.

[48] SF Biagi. Monte carlo simulation of electron drift and diffusion in counting gases under the influence of electric and magnetic fields. *Nuclear Instruments and Methods in Physics Research Section A: Accelerators,*

Spectrometers, Detectors and Associated Equipment, 421(1-2):234–240, 1999.

[49] Mohamed Rabie and Christian M Franck. Methes: A monte carlo collision code for the simulation of electron transport in low temperature plasmas. *Computer Physics Communications*, 203:268–277, 2016.

[50] MB Zhelezniak, A Kh Mnatsakanian, and Sergei Vasil'evich Sizykh. Photoionization of nitrogen and oxygen mixtures by radiation from a gas discharge. *High Temperature Science*, 20(3):357–362, 1982.

[51] Anne Bourdon, VP Pasko, NY Liu, Sébastien Célestin, Pierre Ségur, and Emmanuel Marode. Efficient models for photoionization produced by non-thermal gas discharges in air based on radiative transfer and the helmholtz equations. *Plasma Sources Science and Technology*, 16(3):656, 2007.

[52] Alejandro Luque, Ute Ebert, Carolynne Montijn, and Willem Hundsdorfer. Photoionization in negative streamers: Fast computations and two propagation modes. *Applied Physics Letters*, 90(8):081501, February 2007.

[53] O. Chanrion and T. Neubert. A PIC-MCC code for simulation of streamer propagation in air. *Journal of Computational Physics*, 227(15):7222–7245, July 2008.

[54] Teunissen J. 3d simulations and analysis of pulsed discharges. *PhD Thesis*, Technische Universiteit Eindhoven, (http://repository.tue.nl/801516).

[55] Xiaoran Li, Siebe Dijcks, Sander Nijdam, Anbang Sun, Ute Ebert, and Jannis Teunissen. Comparing simulations and experiments of positive streamers in air: Steps toward model validation. *Plasma Sources Science and Technology*, August 2021.

[56] Gideon Wormeester, Sergey Pancheshnyi, Alejandro Luque, Sander Nijdam, and Ute Ebert. Probing photoionization: simulations of positive streamers in varying n2: O2-mixtures. *Journal of Physics D: Applied Physics*, 43(50):505201, 2010.

[57] Robert Marskar. 3D fluid modeling of positive streamer discharges in air with stochastic photoionization. *Plasma Sources Science and Technology*, 29(5):055007, May 2020.